

Fig. 18.7. The approach to chemical equilibrium by strange hadrons in hot hadronic matter at temperature $T = 160$, $\mu_b = 450$ MeV – \bar{s} hadrons are shown in (a), whereas s hadrons are shown in (b) [164].

19 Hadron-freeze-out analysis

19.1 Chemical nonequilibrium in hadronization

In the final state, we invariably see many hadronic particles, and naturally we observe their spectra and yields only in restricted domains of phase space. An extra reaction step of ‘hadronization’ is required in order to connect the properties of the fireball of deconfined quark–gluon matter, and the experimental apparatus. In this process, the quark and gluon content of the fireball is transferred into ultimately free-flowing hadronic particles. In hadronization, gluons fragment into quarks, and quarks coalesce into hadrons.

Hadronization of course occurs in all reactions in which final-state hadrons are observed: for example, in high-energy $e^+e^- \rightarrow q\bar{q}$ reactions, we see jets of final-state hadrons carrying the energy and momentum of the two quarks produced. It is not yet clear whether there is a fundamental difference between the hadronization of a thermal fireball and that of a

fast-moving quark. We refer to the process in which a thermal fireball of quarks and gluons turns into hadrons as statistical hadronization. This is an area of nonperturbative strong-interaction physics in rapid development, and this interesting topic could nearly fill a review of the size of this book.

The question we address is that of whether chemical-equilibrium hadron phase space (the so-called ‘hadronic gas’) can be used consistently to describe the physics of thermal hadronization. We first note that the production of entropy is small, or even null, in hadronization of thermal QGP. Color ‘freezes’, and the excess entropy of QGP has to find a way to get away, so any additional production is hindered. We consider the Gibbs–Duham relation for a unit volume, Eq. (10.26), and combine it with the instability condition of dynamic expansion, Eq. (3.31), cast in the form

$$0 = P|_h + (P|_h + \epsilon|_h) \frac{\kappa v_c^2}{1 - v_c^2}. \quad (19.1)$$

The result is

$$\frac{\epsilon}{\sigma}|_h = \left(T|_h + \frac{\mu_b \nu_b}{\sigma} \Big|_h \right) \left(1 + \frac{\kappa v_c^2}{1 - v_c^2} \right). \quad (19.2)$$

Using the energy, E , the entropy S , and the baryon number b as variables, we obtain [222]

$$\frac{E}{S} \Big|_h = (T|_h + \delta T|_h) \left(1 + \frac{\kappa v_c^2}{1 - v_c^2} \right), \quad \delta T = \mu_b \frac{\nu_b}{\sigma} = \frac{\mu_b}{S/b}. \quad (19.3)$$

For the RHIC, we have $\delta T|_h < 0.4$ MeV, considering that $\mu_b < 40$ MeV and $S/b > 100$, whereas at the top SPS energy we have $\mu_b \simeq 200$ –250 MeV and $S/b \simeq 25$ –45, and thus $\delta T|_h \simeq 5$ –8 MeV. Eq. (19.3) shows that

$$\frac{E}{S} \Big|_h > T|_h \quad (19.4)$$

when super-cooling occurs prior to hadronization. Since all three quantities, $E|_h$, $S|_h$, $T|_h$ can be obtained from particle abundances, this condition can be verified. More generally, we can transcribe the Gibbs–Duham relation, Eq. (10.26), to obtain the relation

$$\frac{E}{S} + \frac{PV}{S} = T + \delta T > T. \quad (19.5)$$

Solving for P/ϵ , we obtain

$$\boxed{\frac{P}{\epsilon} = \frac{T + \delta T - E/S}{E/S}}. \quad (19.6)$$

The study of hadron production, which will follow, allows an evaluation of both the freeze-out temperature and the energy per entropy E/S . The Gibbs–Duhem relation in the form Eq. (19.6) determines a key property of the equation of state, the ratio of the pressure to the energy density. We expect to find P/ϵ negative and small in magnitude, in nonequilibrium-sudden hadronization. In an equilibrium transformation, the range $\frac{1}{3} < P/\epsilon < \frac{1}{7}$, see Fig. 11.3 on page 211, is expected, which spans the domain of highly relativistic matter and realistic hadronic gas.

Chemical nonequilibrium is naturally connected to the sudden (statistical) hadronization, which is the favored reaction mechanism in view of the results seen at the RHIC, and also has been applied successfully to explain the results obtained at the top energy at the SPS. The reader should keep in mind that, as the collision energy is reduced, the transverse expansion of the fireball of dense matter diminishes, and, at a sufficiently low collision energy, a more adiabatic hadronization has to occur. In this ‘AGS limit’, some of the signatures of the QGP phase we are discussing in this chapter may be erased.

The word sudden refers to the time hadrons have available, following their formation, to rescatter from other hadrons. The observed high abundances of short-lived hadronic resonances such as $K^*(892)$ [279], which has a natural half life of $\tau_{K^*} \simeq \ln 2/\Gamma_{K^*} = 2.8$ fm, implies that the decay occurs mostly outside of the hadronic environment. Had the decay products undergone rescattering, reconstruction of the $K^*(892)$ would in most cases be impossible. Conversely, reconstruction of abundant $K^*(892)$ implies that the two decay products (π and K) did not propagate through dense hadron matter [224, 260]. The HBT results, section 9.3, also place a very severe constraint on the size and life span of the pion source. The source is smaller than one would expect if the prolonged expanding HG phase were to exist. Finally, the hadron spectra are described in terms of a source breaking up at $T = 165 \pm 7$ MeV and expanding with $v_{\perp} = 0.52c$ [84], with chemical and thermal freeze-outs coinciding.

It has been proposed that a mechanical instability associated with super-cooling of QGP is at the origin of the sudden-breakup mechanism. In section 3.5, we have seen that the motion of the quark–gluon fluid adds to the pressure exercised against the vacuum. Equation (3.31) describes the balance condition when the dynamic expansion has run out of ‘speed’. The normal stable case is that $v_c = 0$. However, if the initial condition generated by the great collisional compression produces a fast expansion with a finite velocity $v_c \neq 0$ when the condition Eq. (3.31) is satisfied, this means that the outward flowing QGP matter is at a pressure $P = P_p - \mathcal{B} < 0$, a highly unstable situation, in the (locally at rest) frame of reference. The fireball matter reaching this super-cooled

condition breaks up into smaller clusters. These drops of QGP separate and hadronize into free-streaming hadrons. A HG phase is never formed. However, production of particles occurs as dictated by the phase space available. Their yields are controlled by abundances of quarks in the hadronizing phase.

19.2 Phase space and parameters

Before proceeding with this section, the reader should refresh his memory about the role chemical potentials play in counting hadrons (sections 11.2 and 11.4). The approach we present is in its spirit a generalization of Fermi's statistical model of hadron production [121, 122], in that the yield of hadrons is solely dictated by the study of the magnitude of the phase space available.

The relative number of final-state hadronic particles freezing out from, e.g., a thermal quark–gluon source, is obtained by noting that the fugacity f_i of the i th emitted composite hadronic particle containing k components is derived from fugacities λ_k and phase-space occupancies γ_k :

$$N_i \propto e^{-E_i/T_f} f_i = e^{-E_i/T_f} \prod_{k \in i} \gamma_k \lambda_k. \quad (19.7)$$

In most cases, we study chemical properties of the light quarks u and d jointly, though, on occasion, we will introduce the isospin asymmetry, Eq. (11.11). As seen in Eq. (19.7), we study particle production in terms of five statistical parameters, T , λ_q , λ_s , γ_q , and γ_s . In addition, to describe the shape of spectra, one needs matter-flow-velocity parameters; these become irrelevant when only total abundances of particles are studied; these are obtained by integrating over all of phase space, or equivalently in the presence of strong longitudinal flow, when we are looking at a yield per unit rapidity.

Assuming a QGP source, several of the statistical parameters have natural values.

1. λ_s . The fugacity of the strange quark λ_s can be obtained from the requirement that strangeness balances, $\langle n_s \rangle - \langle n_{\bar{s}} \rangle = 0$, which, for a source in which all s and \bar{s} quarks are unbound and have symmetric phase space, Eq. (11.13), implies $\lambda_s = 1$. However, the Coulomb distortion of the strange-quark phase space plays an important role in the understanding of this constraint for Pb–Pb collisions, leading to the Coulomb-deformed value $\lambda_s \simeq 1.1$; see section 11.3.
2. γ_s . The strange-quark phase-space occupancy γ_s can be computed, section 17.5, within the framework of kinetic theory and $\gamma_s \simeq 1$. Recall that the difference between the two different types of chemical parameters λ_i and γ_i is that the phase-space-occupancy factor γ_i regulates

the number of pairs of flavor ‘ i ’, and hence applies in the same manner to particles and antiparticles, whereas the fugacity λ_i applies only to particles, while λ_i^{-1} is the antiparticle fugacity.

3. λ_q . The light-quark fugacity λ_q , or, equivalently, the baryo-chemical potential, Eq. (11.2a), regulates the baryon density of the fireball and hadron freeze-out. This density can vary depending on the energy and size of colliding nuclei, and the value of λ_q is not easily predicted. However, it turns out that this is the most precisely measurable parameter, with everybody obtaining the same model-independent answer, for it directly enters all highly abundant hadrons. Since T differs depending on the strategy of analysis, the value of μ_b is not so well determined.
4. γ_q . The equilibrium phase-space occupancy of light quarks γ_q is expected to significantly exceed unity in order to accommodate the excess entropy content in the plasma phase. There is an upper limit, Eq. (7.20). We addressed this in section 7.5.
5. T_f . The freeze-out temperature T_f is expected to be within 10% of the Hagedorn temperature $T_H \simeq 160$ MeV, which characterized the production of particles in proton–proton reactions; see chapter 12.
6. v_c . The collective-expansion velocity v_c is expected to remain near to the relativistic velocity of sound,

$$v_c \leq 1/\sqrt{3},$$

the natural speed of flow of information in the QGP phase. There is a longitudinal velocity, which is needed in order to describe rapidity spectra, section 8.3, and there is a motion of the hadronization surface, aside from many further parameters one may wish to use to model the velocity profile of flowing matter.

The resulting yields of final-state hadronic particles are most conveniently characterized by taking the Laplace transform of the accessible phase space. This approach generates a function that, in terms of its mathematical properties, is identical to the partition function. For example, for the open-strangeness sector, we find (with no flow)

$$\mathcal{L} \left(e^{-E_i/T_f} \prod_{k \in i} \gamma_k \lambda_k \right) \propto \ln \mathcal{Z}_s^{\text{HG}}, \quad (19.8)$$

with $\ln \mathcal{Z}_s^{\text{HG}}$ given in Eq. (11.19).

It is important to keep in mind that

- Eq. (19.8) does not require formation of a phase comprising a gas of hadrons, but is not inconsistent with such a step in the evolution of the

matter; Eq. (19.8) describes not a partition function, but just a look-alike object arising from the Laplace transform of the accessible phase space;

- the final abundances of particles measured in an experiment are obtained after all unstable hadronic resonances ‘ j ’ have been allowed to disintegrate, contributing to the yields of stable hadrons; and
- in some experimental data, it is important to distinguish between the two light-quark flavors, for example experiments are sensitive only to Ξ^- , not to Ξ^0 , and averaging over isospin does not occur.

The unnormalized particle multiplicities arising are obtained by differentiating Eq. (19.8) with respect to the particle fugacity. The relative particle yields are simply given by ratios of corresponding chemical factors, weighted by the size of the momentum phase space accepted by the experiment. The ratios of strange antibaryons to strange baryons *of the same type of particles* are, in our approach, simple functions of the quark fugacities; see Eqs. (11.21a)–(11.21e). When particles of unequal mass are considered, and are fed by decay of other hadrons, considerable numerical effort is required to evaluate yield ratios for particles, in particular, if these are available in a fraction of phase space only. To the best of our knowledge, the numerical results of various groups working with the statistical-hadronization method are consistent, though the physics content can vary widely, depending on assumptions introduced.

19.3 SPS hadron yields

We have argued that, in general, we must expect $\gamma_q \neq 1$, section 19.1, i.e., chemical nonequilibrium at hadron freeze-out is an expected ingredient in a precise interpretation of the experimental results on particle ratios obtained in the SPS energy range. For strangeness, it has been expected and was seen early on in experimental data [216]. Full chemical nonequilibrium was first noted in the study of the S–Au/W/Pb collisions at 200A GeV [176]. On fitting the yields of hadrons observed, it was noted that the statistical significance increased when chemical nonequilibrium was introduced. The statistical significance is derived from the total statistical error:

$$\chi^2 \equiv \frac{\sum_j (R_{\text{th}}^j - R_{\text{exp}}^j)^2}{(\Delta R_{\text{exp}}^j)^2}. \quad (19.9)$$

It is common to normalize χ^2 by the difference between the number of data points and parameters used, the so-called ‘dof’ (degrees-of-freedom) quantity.

Table 19.1. Statistical parameters obtained from fits of data for S–Au/W/Pb collisions at 200A GeV, without enforcing conservation of strangeness [176]

T_f [MeV]	λ_q	λ_s	γ_s	γ_q	χ^2/dof
145 ± 3	1.52 ± 0.02	1*	1*	1*	17
144 ± 2	1.52 ± 0.02	0.97 ± 0.02	1*	1*	18
147 ± 2	1.48 ± 0.02	1.01 ± 0.02	0.62 ± 0.02	1*	2.4
144 ± 3	1.49 ± 0.02	1.00 ± 0.02	0.73 ± 0.02	1.22 ± 0.06	0.90

* denotes fixed (input) values

We show the resulting statistical parameters obtained in hadron-yield fits in table 19.1, for S–Au/W/Pb collisions at 200A GeV. Asterisks (*) mark fixed (input) values, thus the first column assumes not only chemical equilibrium, but also the symmetric value $\lambda_s = 1$ for the QGP phase space. Interestingly, little is gained by allowing λ_s to vary, and all different fitting strategies point to $\lambda_s = 1$. However, allowing for strange $\gamma_s \neq 1$ and then light-quark $\gamma_q \neq 1$, nonequilibrium brings the result of the fit progressively to statistical significance. For systems we study, with a few degrees of freedom (typically 5–15), a statistically significant fit requires that $\chi^2/\text{dof} < 1$. For just a few ‘dof’, the error should be as small as $\chi^2/\text{dof} < 0.5$. The usual requirement $\chi^2 \rightarrow 1$ applies only for infinitely large ‘dof’. We learn from these results that the chemical nonequilibrium factor γ_i for both strange and light quarks is a required ingredient in the statistical hadronization model.

Turning now to the Pb–Pb system at collision energy 158A GeV, we consider the particles listed in the top section of table 19.2 from the experiment WA97, for $p_\perp > 0.7$ GeV, within a narrow central-rapidity window $\Delta y = 0.5$. Further below are shown results from the large-acceptance experiment NA49, extrapolated by the collaboration to full 4π coverage of phase space. The total error χ^2 for the two columns of results is shown at the bottom of this table along with the number of data points ‘ N ’ and parameters ‘ p ’ used, and the number of (algebraic) redundancies ‘ r ’ connecting the experimental results. For $r \neq 0$, it is more appropriate to quote the total χ^2 , since the condition for statistical relevance is more difficult to establish given the constraints, but since $\chi^2/(N - p - r) < 0.5$, we are certain to have a valid description of hadron multiplicities. We will return to discuss the yields of Ω and $\bar{\Omega}$ at the end of this section.

In table 19.2 second from last column, the superscript ‘s’ means that λ_s is fixed by strangeness balance. The superscript ‘ γ_q ’, in the two last columns means that $\gamma_q = \gamma_q^c = e^{m_\pi/(2T_f)}$ is fixed in such a way as to maximize the entropy content in the hadronic phase space. The fits presented were obtained with the updated NA49 experimental results, i.e., they include the updated h^-/b , newly published yield of ϕ [43], and pre-

Table 19.2. WA97 (top) and NA49 (bottom) Pb–Pb 158A-GeV-collision hadron ratios compared with phase-space fits

Ratios	Reference	Experimental data	Pb ^{s,γ_q}	Pb ^{γ_q}
Ξ/Λ	[171]	0.099 ± 0.008	0.096	0.095
$\bar{\Xi}/\bar{\Lambda}$	[171]	0.203 ± 0.024	0.197	0.199
$\bar{\Lambda}/\Lambda$	[171]	0.124 ± 0.013	0.123	0.122
$\bar{\Xi}/\Xi$	[171]	0.255 ± 0.025	0.251	0.255
K^+/K^-	[79]	1.800 ± 0.100	1.746	1.771
K^-/π^-	[248]	0.082 ± 0.012	0.082	0.080
K_s^0/b	[152]	0.183 ± 0.027	0.192	0.195
h^-/b	[43]	1.970 ± 0.100	1.786	1.818
ϕ/K^-	[21]	0.145 ± 0.024	0.164	0.163
Λ/\bar{p}	$y = 0$		0.565	0.568
\bar{p}/π^-	All y		0.017	0.016
	χ^2		1.6	1.15
	$N; p; r$		9; 4; 1	9; 5; 1

dict the $\bar{\Lambda}/\bar{p}$ ratio. b is here the number of baryon participants, and $h^- = \pi^- + K^- + \bar{p}$ is the yield of stable negative hadrons, which includes pions, kaons, and antiprotons. We see, on comparing the two columns, that conservation of strangeness (which is enforced in the second from last column) is consistent with the experimental data shown; enforcing it does not change much the results for particle multiplicities.

The six parameters ($T, v_c, \lambda_q, \lambda_s, \gamma_q$ and γ_s) describing the abundances of particles are shown in the top section of table 19.3. Since the results of the WA97 experiment do not cover the full phase space, one finds a reasonably precise value for one velocity parameter, taken to be the spherical surface-flow velocity v_c of the fireball hadron source.

As in S-induced reactions in which $\lambda_s = 1$ [176], so also in Pb-induced reactions, a value $\lambda_s^{Pb} \simeq 1.1$ characteristic of a source of freely movable strange quarks with balancing strangeness, i.e., with $\bar{\lambda}_s = 1$, is obtained; see Eq. (11.17). Since all chemical-nonequilibrium studies of the Pb–Pb system converge to the case of maximum entropy, see Fig. 7.7 on page 125, we have presented the results with fixed $\gamma_q = \gamma_q^c = e^{m_\pi/(2T_f)}$. The large values of $\gamma_q > 1$ seen in table 19.3 confirm the need to hadronize the excess entropy of the QGP that possibly is formed. This value is derived both from the specific abundance of negative hadrons h^-/b and from the relative yields of strange hadrons.

The results shown in table 19.3 allow us to evaluate P/ϵ , section 19.1. Using Eq. (19.6) with $\delta T = 8$ MeV (see Eq. (19.3)), $T = 148$ MeV, and

Table 19.3. Upper section; the statistical model parameters which best describe the experimental results for Pb–Pb data seen in table 19.2; bottom section, energy per entropy, antistrangeness, and net strangeness of the full hadron phase space characterized by these statistical parameters. In column two, we fix λ_s by the requirement of conservation of strangeness

	Pb $_v^{s,\gamma_q}$	Pb $_v^{\gamma_q}$
T [MeV]	151 ± 3	147.7 ± 5.6
v_c	0.55 ± 0.05	0.52 ± 0.29
λ_q	1.617 ± 0.028	1.624 ± 0.029
λ_s	1.10*	1.094 ± 0.02
γ_q	$\gamma_q^{c*} = e^{m_\pi/(2T_f)} = 1.6$	$\gamma_q^{c*} = e^{m_\pi/(2T_f)} = 1.6$
γ_s/γ_q	1.00 ± 0.06	1.00 ± 0.06
E/b [GeV]	4.0	4.1
s/b	0.70 ± 0.05	0.71 ± 0.05
E/S [MeV]	163 ± 1	160 ± 1
$(\bar{s} - s)/b$	0*	0.04 ± 0.05

* indicates values resulting from constraints.

$E/S = 160$ MeV, we obtain $P/\epsilon \sim -1/40$. This negative and small value is consistent with the super-cooling hypothesis. One other interesting quantitative results of this analysis is shown in the bottom section of table 19.3: the yield of strangeness per baryon, $s/b \simeq 0.7$. We see, in the lower portion of table 19.3, that near strangeness balance is obtained without constraint.

The most rarely produced hadrons are the triply strange $\Omega(sss)$ and $\bar{\Omega}(\bar{s}\bar{s}\bar{s})$, which are the heaviest stable hadrons, $M_\Omega = 1672$ MeV. The phase space for $\bar{\Omega}$ is ten times smaller than that for $\bar{\Xi}$ under the conditions of chemical freeze-out we have obtained, and any contribution from non-statistical hadronization would be visible first in the pattern of production of Ω and $\bar{\Omega}$. For the parameters in table 19.3, the yields of $\bar{\Omega}$ reported for the experiment WA97 are underpredicted by nearly a factor of two. This excess yield originates at the lowest m_\perp , as can be seen in Fig. 8.11 on page 155. The ‘failure’ of a statistical-hadronization model to describe yields of $\bar{\Omega}$ (and, by 30%, Ω) has several possible explanations.

One is the possibility that an enhancement in production of Ω and $\bar{\Omega}$ is caused by pre-clustering of strangeness in the deconfined phase [215]. This would enhance the production of all multistrange hadrons, but most prominently the phase-space-suppressed yields of Ω and $\bar{\Omega}$. This mechanism would work only if pairing of strange quarks near to the phase transition were significant. Current models of ‘color superconductivity’ support such a clustering mechanism [30, 185, 206, 237]. We have men-

tioned, at the end of section 11.5, the possibility that distillation of strangeness followed by breakup of strangelets could contribute to production of Ω and $\bar{\Omega}$. The decay of disoriented chiral condensates has also been proposed as a source of soft Ω and $\bar{\Omega}$ [158].

A more conventional explanation for the excess production of Ω and $\bar{\Omega}$ is obtained by noting that, due to the low reaction cross section, Ω and $\bar{\Omega}$ could decouple from the HG background somewhat sooner than do all the other hadrons [55, 263]. To augment the yields by factor k , it is sufficient to take an incrementally δT_Ω higher freeze-out temperature, determined from studying the Ω phase space:

$$\delta T_\Omega \simeq T \frac{\ln k}{M_\Omega/T}. \quad (19.10)$$

In order to increase the yield by a factor of two, the freeze-out of Ω would need to occur at $T_\Omega = 160$ MeV rather than at $T = 150$ MeV. Since the temperature drops as the expansion of the fireball develops, a higher freeze-out temperature means freeze-out occurring slightly earlier in time. Even though the required staging in time of hadron production is apparently small, a consistent picture requires fine-tuning and it seems unnatural, considering that yields of all the other particles are perfectly consistent with just one sudden chemical-freeze-out condition.

In view of these pre- and post-dictions of the anomalous yield of Ω and $\bar{\Omega}$, one should abstain from introducing these particles into statistical-hadronization-model fits. We note that the early statistical descriptions of yields of Ω and $\bar{\Omega}$ have not been sensitive to the problems we described [61, 180]. In fact, as long as the parameter γ_q is not considered, it is not possible to describe the experimental data at the level of precision that would allow recognition of the excess yield of Ω and $\bar{\Omega}$ within statistical hadronization model. For example, a chemical-equilibrium fit, which includes the yield of Ω and $\bar{\Omega}$ has for 18 fitted data points with two parameters a $\chi^2/\text{dof} = 37.8/16$ [80]. Such a fit is quite unlikely to contain all the physics even if its appearance to the untrained eye suggests that a very good description of experimental data as been achieved.

19.4 Strangeness as a signature of deconfinement

We have found that the rate of production of strangeness in QGP is sensitive to the temperature achieved at the time gluons reach chemical and thermal equilibrium. There is considerable uncertainty regarding how short the time required to relax the strangeness flavor in the thermal gluon medium is, with the upper limit being the hatched area in Fig. 17.11. Consideration of the small mass for strangeness found in lattice studies of strange hadrons has yielded much smaller τ_s (the thin-dotted line in

Fig. 17.11). There is also the probable further reduction due to the next-to-leading-order effects (the K -factor). In view of this, we now establish a benchmark yield of strangeness, assuming that the equilibration process leads to near-chemical-equilibrium conditions for hadronizing QGP. Specifically, the abundance of light quarks in the QGP phase may be considered near to the equilibrium yield, $\gamma_q^{\text{QGP}} \rightarrow 1$, whereas the yield of strange quarks characterized by the QGP phase-space occupancy before hadronization, γ_s^{QGP} , may differ appreciably from equilibrium.

We consider the ratio of the equilibrium density of strangeness, arising in the Boltzmann-gas limit, Eq. (10.51), to the baryon density in a fireball of QGP given in Eq. (10.75):

$$\frac{\rho_s}{\rho_b} = \frac{s}{b} = \frac{s}{q/3} = \frac{\gamma_s^{\text{QGP}} (3/\pi^2) T^3 W(m_s/T)}{\gamma_q^{\text{QGP}} \frac{2}{3} (\mu_q T^2 + \mu_q^3/\pi^2)}. \tag{19.11}$$

W is as defined in Eq. (10.50a) and shown in Fig. 10.1. The equilibrium strange-quark density Eq. (10.51), with $g_s = 6$, is the first term in the expansion Eq. (10.63). Higher-order quantum-statistics correction terms are negligible, given $m_s/T = \mathcal{O}(1)$. To a first approximation, perturbative thermal QCD corrections, see Eq. (16.24), cancel out in the ratio. For $m_s = 200$ MeV and $T = 150$ MeV, we have

$$\frac{s}{b} \simeq \frac{\gamma_s^{\text{QGP}}}{\gamma_q^{\text{QGP}}} \frac{0.7}{\ln \lambda_q + (\ln \lambda_q)^3/\pi^2}. \tag{19.12}$$

The relative yield s/b is mainly dependent on the value of λ_q . In the approximation considered, it is nearly temperature-independent. This light-quark fugacity pertinent to the final-state hadrons is well determined and does not vary depending on the strategy used for analysis of data.

We show in Fig. 19.1, as a function of $\lambda_q - 1$ (the variable chosen to enlarge the interesting region $\lambda_q \rightarrow 1$), the expected relative yield per baryon originating from the QGP, defined in Eq. (19.12) with $\gamma_s^{\text{QGP}} = \gamma_q^{\text{QGP}} = 1$. At the top SPS energy, we see that the equilibrium yield is 1.5 pairs of strange quarks per participating baryon (for $\lambda_q \simeq 1.5$ –1.6). Considering the experimental yield in table 19.3, $\gamma_s^{\text{QGP}} \sim 0.5$. The explanation of this is that, if formed, the QGP system did not become hot enough for long enough. In p–p collisions at the corresponding energy, the yield is below 0.3 pairs of strange quarks per participant [277], which is 40% of the Pb–Pb yield.

For the RHIC 130-GeV run, the value $\lambda_q = 1.09$ allows one to understand many particle yields at central rapidity. We see, in Fig. 19.1, that the specific yield of strangeness in a fireball of QGP at equilibrium is an order of magnitude greater than that currently observed at the SPS top

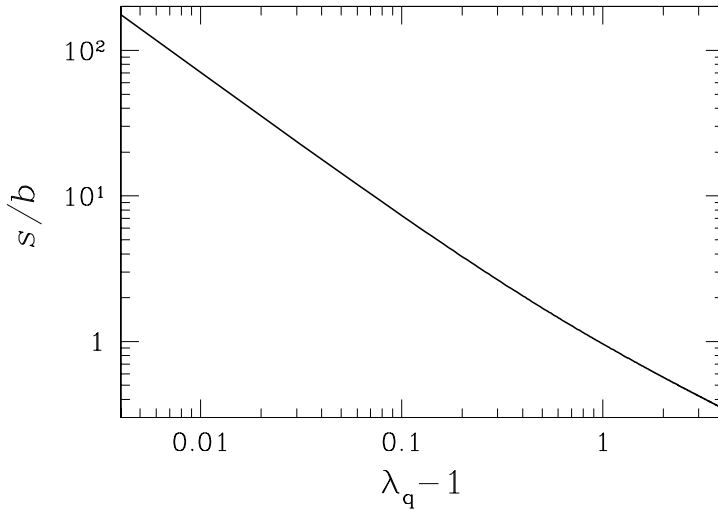


Fig. 19.1. The yield of strangeness per baryon as a function of λ_q in equilibrated QGP.

energy. This remarkable increase is due to the expected chemical equilibration ($\gamma_s \rightarrow 1$) at the RHIC, see section 17.5, as well as to a substantial reduction of baryon density at central rapidity. In comparison with the general hadron multiplicity, only a modest enhancement of production of strangeness at most can be expected at the RHIC, compared to SPS; the remarkable feature of the RHIC situation is that this enhancement is found in the abundance of (multi)strange baryons. Given the large strangeness-per-baryon ratio, baryons and antibaryons produced at the RHIC are mostly strange [221]. We are not aware of any reaction model other than formation of QGP and its hadronization that could produce this type of yield anomaly.

While the specific yield of strangeness s/b is a clear indicator for the extreme conditions reached in heavy-ion collisions, a more directly accessible observable is the occupancy of the hadron-strangeness phase space, γ_s^{HG} . Due to the need to hadronize into a strangeness-poor phase, γ_s^{HG} can be appreciably greater than unity. To understand this, we compare the phase space of strangeness in QGP with that of the resulting HG. The absolute yields must be the same in both phases. This hadronization condition allows us to relate the two phase-space occupancies in HG and QGP, by equating the strangeness content in the two phases. On canceling out the common normalization factor $T^3/(2\pi^2)$, Eq. (11.26), we obtain

$$\gamma_s^{\text{QGP}} V^{\text{QGP}} g_s W\left(\frac{m_s}{T^{\text{QGP}}}\right) \simeq \gamma_s^{\text{HG}} V^{\text{HG}} \left(\frac{\gamma_q \lambda_q}{\lambda_s} F_K + \frac{\gamma_q^2}{\lambda_q^2 \lambda_s} F_Y \right). \quad (19.13)$$

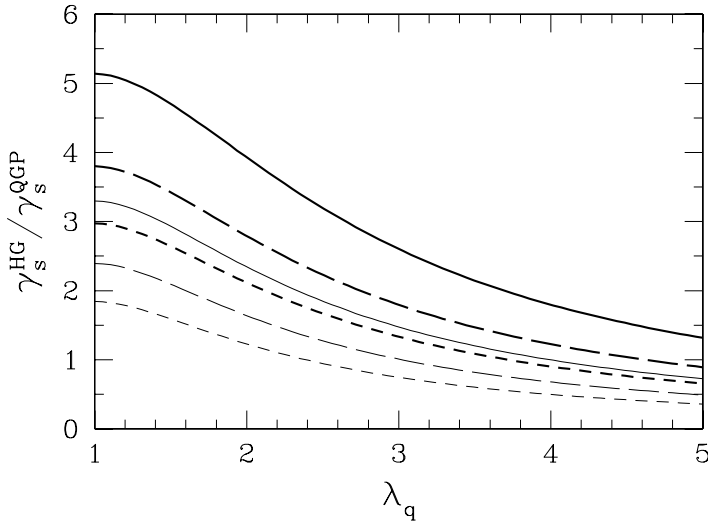


Fig. 19.2. The HG/QGP strangeness-occupancy γ_s ratio in sudden hadronization as a function of λ_q . Solid lines, $\gamma_q^{\text{HG}} = 1$; long-dashed lines, $\gamma_q^{\text{HG}} = 1.3$; and short-dashed lines, $\gamma_q^{\text{HG}} = 1.6$. Thin lines are for $T = 170$ and thick lines for $T = 150$ MeV, for both phases.

Here we have, without loss of generality, followed the \bar{s} -carrying hadrons in the HG phase space, and we have omitted the contribution of multistrange antibaryons for simplicity. We now use the condition that strangeness is conserved, Eq. (11.28), to eliminate λ_s from Eq. (19.13), and obtain

$$\frac{\gamma_s^{\text{HG}} V^{\text{HG}}}{\gamma_s^{\text{QGP}} V^{\text{QGP}}} = \frac{g_s W(m_s/T^{\text{QGP}})}{\sqrt{(\gamma_q F_K + \gamma_q^2 \lambda_q^{-3} F_Y)(\gamma_q F_K + \gamma_q^2 \lambda_q^3 F_Y)}}. \tag{19.14}$$

In sudden hadronization, $V^{\text{HG}}/V^{\text{QGP}} \simeq 1$, the growth of volume is negligible, $T^{\text{QGP}} \simeq T^{\text{HG}}$, the temperature is maintained across the hadronization front, and the chemical occupancy factors in both states of matter accommodate the different magnitude of the particle phase space. In this case, the ‘squeezing’ of the strangeness of the QGP into the smaller HG phase space results in $\gamma_s^{\text{HG}}/\gamma_s^{\text{QGP}} > 1$. We show, in Fig. 19.2, the enhancement of phase-space occupancy expected in sudden hadronization of the QGP. The temperature ranges $T = 150$ MeV (thick lines) and $T = 170$ MeV (thin lines) span the ranges being considered today at the SPS and RHIC. The value of γ_q is in the range of the chemical equilibrium in HG, $\gamma_q = 1$ (solid lines), to the expected excess in sudden hadronization, see section 7.5, $\gamma_q = 1.6$ (short-dashed lines), with the intermediate value $\gamma_q = 1.3$ (long-dashed lines).

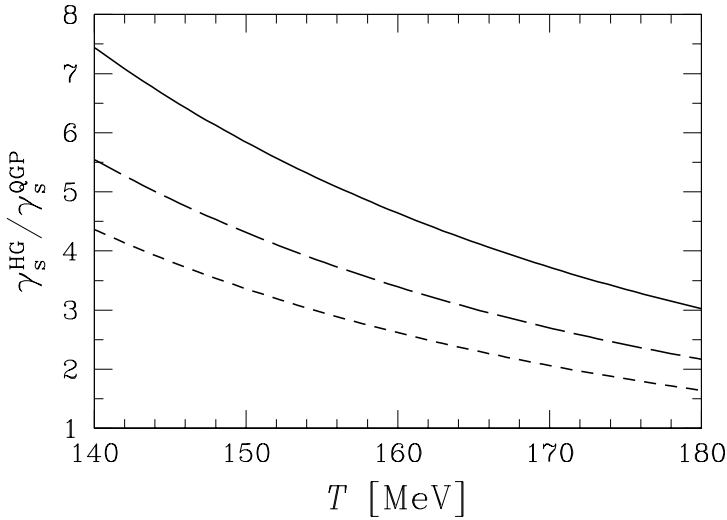


Fig. 19.3. The HG/QGP strangeness-occupancy γ_s ratio in sudden hadronization, as a function of T for $\lambda_q = 1$. Solid line, $\gamma_q^{\text{HG}} = 1$; long-dashed line, $\gamma_q^{\text{HG}} = 1.3$; and short-dashed line, $\gamma_q^{\text{HG}} = 1.6$.

We note that, for the top SPS energy range, for which $\lambda_q = 1.5$ – 1.6 , sudden-hadronization analysis of data implies $T \simeq 150$ MeV and $\gamma_q \simeq 1.6$, and the value of γ_s increases across hadronization by factor 2.7. Since the yield of strangeness seen at the SPS implies that $\gamma_s^{\text{QGP}} \simeq 0.6$, this in turn implies that $\gamma_s^{\text{HG}} \simeq 1.6 \simeq \gamma_q^{\text{HG}}$, as is indeed found in hadron-production analysis in the sudden-hadronization picture; see table 19.3.

Because $\gamma_s^{\text{HG}} / \gamma_q^{\text{HG}} \simeq 1$, one can also model the hadronization at the SPS energy in terms of an equilibrium-hadronization model. The enhancement in production of pions associated with the high-entropy phase can be accommodated by use of two temperatures, one for the determination of absolute yields of particles, and another for determination of the spectral shape. Such an approach has a similar number of parameters, and comparable predictive power. However, the SPS condition, $\gamma_s^{\text{HG}} / \gamma_q^{\text{HG}} \simeq 1$, does not hold for the RHIC energy range. We therefore expect that a much clearer picture about the dynamics of hadronization of QGP should emerge from the study of yields of strange particles at the RHIC.

As can be seen in Fig. 19.2, near $\lambda_q \rightarrow 1$ (the condition at the RHIC) there is practically no variation in the ratio $\gamma_s^{\text{HG}} / \gamma_q^{\text{HG}}$. Therefore, we consider, in Fig. 19.3 for $\lambda_q = 1$, the dependence on the hadronization temperature of $\gamma_s^{\text{HG}} / \gamma_q^{\text{HG}}$, with the three cases shown: solid line, $\gamma_q = 1$; long-dashed line, $\gamma_q = 1.3$; and short-dashed line, $\gamma_q = 1.6$. We now compare the hadronization conditions for the RHIC in the range between

$T = 180$ MeV and $\gamma_q = 1$ and $T = 155$ MeV and $\gamma_q = 1.6$. Across this domain, we see that the phase space of strangeness in the HG is three times smaller than that in QGP, or, as shown in Fig. 19.3, there is this large increase in occupancy of the strange-quark phase space.

In the likely event that the QGP formed at the RHIC evolves toward the chemical-equilibrium abundance of strangeness, or possibly even exceeds it, section 17.5, we should expect a noticeable over-occupancy of strangeness to be measured in terms of the chemical-equilibrium abundance of final-state hadrons. This high phase-space occupancy is one of the requirements for the enhancement of production of multistrange (anti)baryons, which is an important hadronic signal of QGP phenomena [213–215, 226]. In particular, we hope that hadrons produced in phase space with a small probability, such as Ω and $\bar{\Omega}$, will be observed with yields above expectations, continuing the trend seen at the SPS. Because much of the strangeness is in the baryonic degrees of freedom, the kaon-to-pion ratio appears suppressed, in Fig. 1.5 on page 17, relative to SPS results, however we will show below that this is not the case.

Many results from the RHIC run at $\sqrt{s_{NN}} = 130$ GeV are still preliminary and the following quantitative discussion is probably not the final word on this matter. However, the results we find are very interesting, and in qualitative agreement with the sudden-breakup reaction picture of QGP predominantly presented in this book. The data is mainly obtained in the central-rapidity region, where, due to approximate longitudinal scaling, the effects of flow cancel out and we can evaluate the full phase-space yields in order to obtain particle ratios. We do not explore trivial results such as $\pi^+/\pi^- = 1$, since the large hadron yield combined with the flow of baryon isospin asymmetry toward the fragmentation rapidity region assures us that this result will occur to within a great precision. We also do not use the results for K^* and \bar{K}^* since these yields depend on the degree of rescattering of resonance decay products [224, 259]. The data we use has been reported in conference reports of the STAR collaboration of summer 2001, which has been combined with data of PHENIX, BRAHMS, and PHOBOS; for more discussion of the origin of data, see [81]. We assume, in our fit in table 19.4, that the multistrange weak-interaction cascading $\Xi \rightarrow \Lambda$, in the STAR result we consider, is cut by vertex discrimination and thus we use these uncorrected yields.

We first look at the last column in table 19.4, the chemical-equilibrium fit. Its large χ^2 originates from the inability to account for production of multistrange Ξ and Ξ . Similar results are presented in [81], in an equilibrium fit that does not include multistrange hadrons. The equilibrium fit yields $E/S = 159$ MeV $< T = 183$ MeV. With a negligible contribution from δT , Eq. (19.6) implies that $P/\epsilon \simeq 1/6.6$ as is expected for the high-freeze-out temperature.

Table 19.4. Fits of central-rapidity hadron ratios for the RHIC run at $\sqrt{s_{NN}} = 130$ GeV. Top section: experimental results, followed by chemical parameters, physical properties of the phase space, and the fitting error. Columns: data, the full nonequilibrium fit, the nonequilibrium fit constrained by conservation of strangeness and supersaturation of pion phase space, and, in the last column, the equilibrium fit constrained by conservation of strangeness, superscript * indicates quantities fixed by these considerations

	Data	Fit	Fit	Fit ^{eq}
			$s - \bar{s} = 0$	$s - \bar{s} = 0$
\bar{p}/p	0.64 ± 0.07	0.637	0.640	0.587
\bar{p}/h^-		0.068	0.068	0.075
$\bar{\Lambda}/\Lambda$	0.77 ± 0.07	0.719	0.718	0.679
Λ/h^-	0.059 ± 0.001	0.059	0.059	0.059
$\bar{\Lambda}/h^-$	0.042 ± 0.001	0.042	0.042	0.040
Ξ/Ξ	0.83 ± 0.08	0.817	0.813	0.790
Ξ^-/Λ	0.195 ± 0.015	0.176	0.176	0.130
$\Xi^-/\bar{\Lambda}$	0.210 ± 0.015	0.200	0.200	0.152
K^-/K^+	0.88 ± 0.05	0.896	0.900	0.891
K^-/π^-	0.149 ± 0.020	0.152	0.152	0.145
K_S/h^-	0.130 ± 0.001	0.130	0.130	0.124
Ω/Ξ^-		0.222	0.223	0.208
$\bar{\Omega}/\Xi^-$		0.257	0.256	0.247
$\bar{\Omega}/\Omega$		0.943	0.934	0.935
T		158 ± 1	158 ± 1	183 ± 1
γ_q		1.55 ± 0.01	1.58 ± 0.08	1*
λ_q		1.082 ± 0.010	1.081 ± 0.006	1.097 ± 0.006
γ_s		2.09 ± 0.03	2.1 ± 0.1	1*
λ_s		1.0097 ± 0.015	1.0114^*	1.011^*
E/b [GeV]		24.6	24.7	21
s/b		6.1	6.2	4.2
S/b		151	152	131
E/S [MeV]		163	163	159
χ^2/dof		$2.95/(10 - 5)$	$2.96/(10 - 4)$	$73/(10 - 2)$

The chemical-nonequilibrium fit appears more internally consistent. The value of the hadronization temperature $T = 158$ MeV is below the central expected equilibrium phase-transition temperature for the case of $2 + 1$ flavors, section 15.5. This is also near to the $P = 0$ condition for the quark-gluon-liquid model developed in chapter 16, see Fig. 4.2 on page 70, and, as is appropriate, a little above the temperatures seen for the SPS baryon-rich freeze-out; see table 19.3. We find, Eq. (19.6) $P/\epsilon \simeq -1/33$, a value consistent with super-cooling and sudden QGP hadronization. This reaction picture is in agreement with the relatively large γ_s and $\gamma_q > 1$

obtained. Comparing the two types of results, we conclude that it is the inclusion of the yields of the multistrange antibaryons in the RHIC data analysis, along with the hypothesis of chemical nonequilibrium, which allows us to discriminate between the different scenarios of reaction.

We look next at the strangeness content, $s/b = 6$, in table 19.4: the full QGP phase space would have yielded 8.6 pairs of strange quarks per baryon at $\lambda_q = 1.085$, as is seen in Fig. 19.1, and $\gamma_s^{\text{QGP}} = 6/8.6 = 0.7$. With this value, and using the fitted value $\gamma_s^{\text{HG}} = 2.1$, we compute $\gamma_s^{\text{HG}}/\gamma_s^{\text{QGP}} = 2.1/0.7 = 3$ and, as we see in Fig. 19.3, this is, for $T = 158$ MeV and $\gamma_q = 1.55$, the expected condition for hadronization of QGP.

The fact that the inferred strangeness phase space in QGP is not fully saturated is, on a second careful look, in qualitative agreement with predictions of kinetic theory, Fig. 17.13. Namely, particle multiplicities observed and the shape of particle spectra suggest that the initial conditions are near $T = 300$ MeV in the RHIC run at $\sqrt{s_{\text{NN}}} = 130$ GeV, which pushes the value of γ_s^{QGP} , shown in Fig. 17.13, toward 0.9.

A further reduction in this prediction, more applicable to the highest RHIC energy range, arises since the initial volume of the fireball assumed in order to obtain the result in Fig. 17.13 is up to twice as large as that implied by the RHIC 130A-GeV results. This is understood by considering the total experimental hadron multiplicity entropy, which we can derive from the fitted entropy per baryon, $S/b \simeq 150$. We cannot multiply this by the total number of participants, since many of the 350 participating nucleons are found in the fragmentation regions. If we assume that the central-rapidity fraction is 100 baryons, the central entropy content is 15 000, while the calculations for Fig. 17.13 are based on 38 000 entropy units. Thus, the initial volume of the fireball populating the particle yields in the central-rapidity region is about half that used to obtain the results in Fig. 17.13. A smaller system lives for a shorter time, and, since we are not yet in the regime of full equilibration of strangeness, a smaller value of γ_s^{QGP} than that seen in Fig. 17.13 is expected. Also, the smaller volume of the system is more consistent with the HBT results.

The value of the thermal energy content, $E/b = 25$ GeV, seen in the bottom portion of table 19.4 is also in very good agreement with expectations once we allow for the kinetic-energy content associated with longitudinal and transverse motion. The energy of each particle is ‘boosted’ by the factor $\gamma_{\perp}^v \cosh y_{\parallel}$, see, e.g., Eq. (8.39). For $v_{\perp} = c/\sqrt{3}$, we have $\gamma_{\perp}^v = 1.22$. The range of longitudinal flow is about ± 2.3 rapidity units; see Fig. 9.19. To obtain the the increase in energy due to longitudinal flow, we have to multiply by the average, $\int dy_{\parallel} \cosh y_{\parallel}/y_{\parallel} \rightarrow \sinh(2.3)/2.3 = 2.15$, for a total average increase in energy by factor 2.62, which takes the full energy content to $E^v/b \simeq 65$ GeV as expected.

We now consider what these results imply about the total yield of strangeness in the RHIC fireball. First, we sum up the yield of strange quarks contained in hyperons. Recalling Fig. 2.6 on page 32, we have in singly strange hyperons 1.5 times the yield observed in Λ . Also, accounting for the doubly strange Ξ^- , which are half of all the Ξ , we have

$$\frac{\langle s \rangle_Y}{h^-} = 1.5 \times 0.059 + 2 \times 2 \times 0.195 \times 0.059 = 0.133.$$

Allowing for the unobserved Ω at the theoretical rate, this number increases to $\langle s \rangle_Y/h^- = 0.14$. Repeating the same argument for antihyperons, the result is 0.10. The s and \bar{s} content in kaons is four times that in K_S and thus

$$\frac{\langle s + \bar{s} \rangle}{h^-} = 0.76,$$

with 32% of this yield contained in hyperons and antihyperons. Up to this point, the analysis is practically solely based on direct measurements and established yields of particles.

We now estimate the increase in the ‘strangeness-suppression’ factor W_s , Eq. (18.1). Correcting for the presence of K^- among negatively charged hadrons, and assuming that all three pions are equally abundant, we find

$$\frac{\langle s + \bar{s} \rangle}{\pi^- + \pi^+ + \pi^0} \simeq 0.30.$$

The total number of pions produced comprises pions arising from resonance decays and from fragments of the projectile and target. Thus, as few as half of the pions originate from the newly made $q\bar{q}$ pairs. In the RHIC run at $\sqrt{s_{NN}} = 130$ GeV, we estimate $W_s \simeq 0.6$. The increase compared with the SPS energy is largely due to the strangeness content in hyperons. Considering that $\gamma_s^{\text{QGP}} \simeq 0.7$ at $\sqrt{s_{NN}} = 130$ GeV, there is still space for a further rise in yield of strangeness at the highest RHIC energy, and we hope and expect that $W_s \rightarrow 1$ when the initial temperature rises to well above the mass of the strange quark for a sufficient length of time.

We have learned to appreciate, in this last part, how the deconfined thermal phase, through its gluon content, manifests itself as a strangeness signature of QGP. The presence of gluons is essential for rapid thermal production of strangeness. The SPS strangeness results decisively show interesting new physics, with a significant excess of strangeness and strange antibaryons. We see, at the SPS and at the RHIC, considerable convergence of the understanding of the production of hadrons around properties of suddenly hadronizing entropy and strangeness-rich QGP. We see hadronization into pions, at $\gamma_q \rightarrow \gamma_q^c = e^{m_\pi/(2T_f)} \simeq 1.6$, which is

an effective way to convert the excess of entropy in the deconfined state into hadrons. We have seen that strange-particle signatures of hadronization of QGP become more extreme and clearer at the RHIC.

It is important to remember that it is not only at the RHIC, and in the near future at the LHC, that QGP can be studied. An alternative energy domain for investigating QGP is the phase-transition region at high baryon density. It is very probable that the onset of deconfinement occurs at modest collision energies, perhaps in collisions of 20–40 A-GeV Pb projectiles with a laboratory target. The formation of the QGP phase is an endothermic process. In experiments near to the condition for phase transformation, energy balance, lack of explosive flow, and the onset of abundant production of entropy and strangeness as a function of the energy and reaction volume should provide good global signatures of new physics. Anomalous production of multistrange baryons and antibaryons should help to pinpoint the deconfined phase.

We hear sometimes the following question: “Where is the ‘smoking gun’ signature of QGP?”. The disappearance of the suppression of the production of strangeness is surely one such observation. However, we must remember that the discovery of QGP, unlike the discovery of a new particle, requires a change in our understanding of the fundamental hadronic degrees of freedom. This is a deductive process, and requires a global cross check of consistency at each step in its development. It is unlikely that our detailed arguments will persuade the skeptic, however, we hope to show the new way to the uninitiated.

QGP discovery is similar to the slow and painful path to the understanding of electricity. The reader is invited to think through how he/she would proceed without the plug in the wall, the instrument in the laboratory, and the battery in the drawer, and without comprehension of the principles of conductivity, to introduce in a lecture the discovery of the existence of electricity. The challenge of understanding the ‘ionized’ quark–gluon form of matter is certainly more complex than the unraveling of electricity.